HHS Public Access

Author manuscript

Dev Cell. Author manuscript; available in PMC 2024 November 06.

Published in final edited form as:

Dev Cell. 2023 November 06; 58(21): 2195–2205.e5. doi:10.1016/j.devcel.2023.08.003.

Control of Murine Brown Adipocyte Development by GATA6

Seoyoung Jun[1,2,3,4], **Anthony R. Angueira**[2,3,4], **Ethan C. Fein**[2,3,4], **Josephine M. E. Tan**[2,3], **Angela H. Weller**[2,3], **Lan Cheng**[2,3], **Kirill Batmanov**[2], **Jeff Ishibashi**[2,3], **Alexander P. Sakers**[2,3], **Rachel R. Stine**[2,3], **Patrick Seale**[2,3,5,*]

[1.] Department of Biology, University of Pennsylvania, Philadelphia, PA, USA, 19104

[2.] Institute for Diabetes, Obesity & Metabolism, Philadelphia, PA, USA, 19104

[3.] Department of Cell and Developmental Biology; Perelman School of Medicine, University of Pennsylvania, Philadelphia, PA, USA, 19104

[4.] Equal contribution

[5.] Corresponding author and lead contact

Summary

Brown adipose tissue (BAT) is a thermogenic organ that protects animals against hypothermia and obesity. BAT derives from the multipotent paraxial mesoderm; however, the identity of embryonic brown fat progenitor cells and regulators of adipogenic commitment are unclear. Here, we performed single-cell gene expression analyses of mesenchymal cells during mouse embryogenesis with a focus on BAT development. We identified cell populations associated with the development of BAT, including *Dpp4*+ cells that emerge at the onset of adipogenic commitment. Immunostaining and lineage tracing studies show that *Dpp4+* cells constitute the BAT fascia and contribute minorly as adipocyte progenitors. Additionally, we identified the transcription factor GATA6 as a marker of brown adipogenic progenitor cells. Deletion of *Gata6* in the brown fat lineage resulted in a striking loss of BAT. Together, these results identify progenitor and transitional cells in the brown adipose lineage and define a crucial role for GATA6 in BAT development.

eTOC blurb

*Correspondence should be addressed to: Patrick Seale, Perelman School of Medicine, University of Pennsylvania, Smilow Center for Translational Research, 3400 Civic Center Blvd, Rm. 12-105, Philadelphia, PA, USA, 19104. Tel: 215-573-8856, sealep@pennmedicine.upenn.edu.

Author Contributions

S.J., A.R.A., E.C.F. and P.S. were responsible for conceptualization, data analysis and writing the manuscript. S.J. and A.R.A. conducted the majority of the experiments. E.C.F. and A.R.A carried out the bioinformatics analyses of scRNAseq datasets. L.C. processed tissue sections for histology and performed immunostaining. J.M.E.T. performed imaging analysis and assisted with experiments. A.H.W. and K.B. performed ChIP analyses. R.R.S. assisted with experiments and writing of the manuscript. A.S. and J.I. developed cell isolation and embryo cell sorting procedures and assisted in preparing cells for sequencing.

Declaration of interests

The authors declare no competing interests.

Jun, *et al.* utilize single-cell RNA sequencing and lineage tracing analyses to identify a presumptive lineage hierarchy for brown adipocytes and closely associated connective tissues. Furthermore, they identify the transcription factor GATA6 as a critical determinant of brown preadipocyte development and BAT formation.

Graphical Abstract:

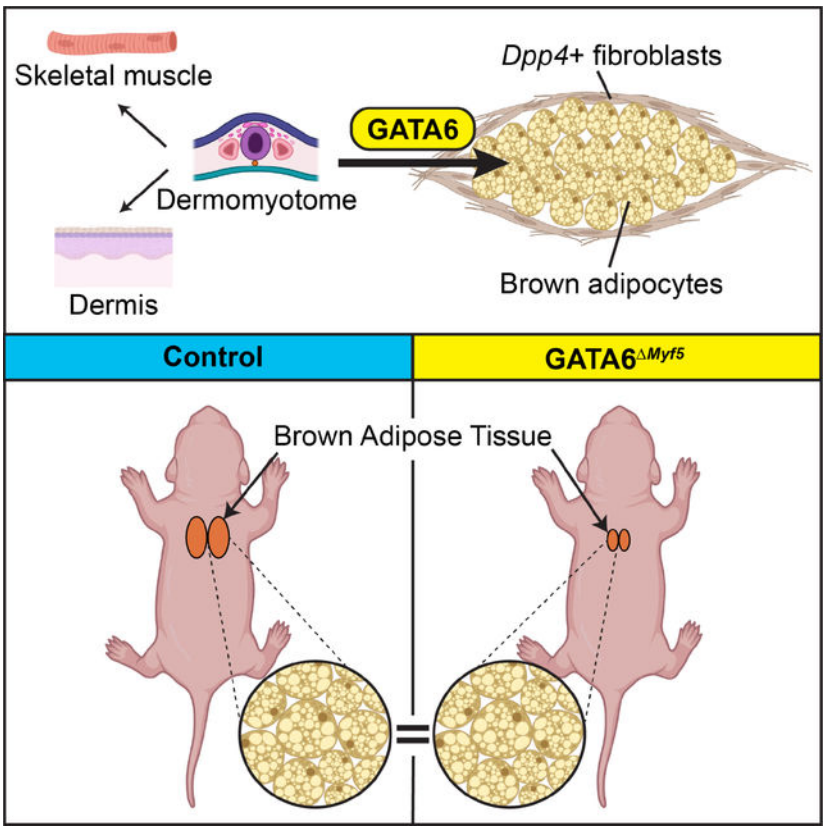

Introduction

Brown adipocytes are specialized to dissipate energy as heat in response to cold exposure, a process known as adaptive thermogenesis. Brown adipocytes localize in discrete deposits of brown adipose tissue (BAT) that develop before or around birth. Thermogenesis in BAT provides a critical source of heat to help animals defend their body temperature during exposure to environmental cold[1,2]. BAT can also contribute to the regulation of body weight and systemic metabolism. Many studies have shown that increasing BAT function in mice protects against obesity and metabolic disease[3,4]. Recent studies also reveal that BAT can suppress or limit tumor growth[5]. Humans possess variable amounts of activate-able BAT, the levels of which correlate with a lean and healthy metabolic phenotype[6–10]. However, humans, especially obese and older people, have relatively low levels of BAT. Thus, BAT-based therapies for obesity and other diseases will require approaches that augment BAT mass, either through increasing native BAT content or through cell transplantation.

A prominent BAT depot develops in the interscapular region of humans and mice[11,12]. Lineage tracing studies in mice indicate that the interscapular BAT along with skeletal muscle, dorsal dermis and subpopulations of white adipocytes descend from the dermomyotome, located in the dorsal region of somites and marked by the expression of *Myf5*, *En1* and *Pax7*[13–17]. Brown adipocytes expressing the master adipogenic factor PPARg are first observed in the interscapular region at about embryonic day 14.5 (E14.5) of development[18,19]. However, the identity, molecular profile and hierarchy of brown adipose progenitor cells are unclear. Moreover, the factors and signaling pathways that control commitment and differentiation of brown adipose cells have not been well studied. A detailed understanding of BAT development could reveal new approaches to increase BAT mass and enable the creation of iPSC-based methods to produce human brown adipocytes for transplantation and analysis.

We utilized scRNA-seq to identify mesenchymal cell types and map cell fate transitions along the paraxial mesoderm-brown fat differentiation trajectory during mouse embryogenesis. These analyses predicted a brown fat lineage hierarchy and identified several stage-specific cell types associated with the differentiation of somitic mesoderm into skeletal muscle, BAT, dermis, and other tissue types. We focused on a cell population that selectively expressed *Dpp4*, shared transcriptional similarity with preadipocytes, and emerged at the onset of brown adipocyte differentiation. Lineage tracing experiments and spatial analyses demonstrated that *Dpp4*+ cells constitute the connective tissue fascia that surrounds BAT lobes and contribute minorly to the development of brown adipocytes. Additionally, we identified the transcription factor GATA6 as a marker gene of brown adipocyte progenitor cells and an essential regulator of BAT development.

Results

Profiling of mesenchymal cells during brown adipose tissue (BAT) development

BAT develops in the interscapular region of mice and humans. To identify cell types that contribute to BAT development, we performed single-cell RNA sequencing (scRNA-seq) analysis of the dorsal anterior region (forelimb level) of mouse embryos at embryonic day (E)10.5 to E15.5 following enrichment of dermomyotome (DM), mesenchymal cells and brown adipose lineage cells (see Methods and Fig. S1 for workflow). We combined and integrated the mesenchymal cell, DM, and skeletal muscle (SkM) clusters from individual time points (Fig. S1A). To refine the analysis, we selected cell clusters predicted by deconvolution analysis to localize to the dorsal mouse embryo in the Mouse Organogenesis Spatial Transcriptomics Atlas (MOSTA)[20] (Fig. S1A). The resulting E10.5-E15.5 dataset illustrated a proposed brown adipose lineage, from DM to differentiated brown adipocytes (Adipo) (Fig. 1A, Fig. S1–S2). Evaluation of the cell profiles by developmental time point indicated that DM and SkM were prominent at E10.5 and E11.5 (Fig. 1B). Mesenchymal cells expressing cadherin-4 (*Cdh4*) with or without nerve growth factor receptor (*Ngfr*) (i.e. *Cdh4*+;*Ngfr*+ and *Cdh4*+;*Ngfr*− cells), preadipocytes (PreAds) and adipocytes (Adipo) were identified at E14.5 (Fig. 1B, S1B). The proportion of adipocytes increased dramatically at E15.5, indicating that this is an active period of adipocyte differentiation and highlighted the efficiency of our enrichment strategy (Fig. 1B).

To identify early BAT progenitor cells deriving directly from the DM, we focused on the developmental stage between E10.5-E13.5, prior to the emergence of PreAds. Here, we identified clusters corresponding to SkM (*Tnnt1*+), DM (*En1*+), dermis (*Twist2*+), and sclerotome (*Pax1*+), as well as cell clusters marked by expression of: *Cdh4* and the brown adipogenic factor, early B cell factor-2 (*Ebf2*) (i.e. *Cdh4*+; *Ebf2*+), empty spiracles homeobox 2 (*Emx2*), or short-stature homeobox (*Shox2*) (Fig. 1C, D). Clusters closely related to DM included SkM and dermis, as expected, but also *Cdh4*+;*Ebf2*+ and *Emx2*+ cells (Fig. 1C, D). Deconvolution analysis of the MOSTA based on our scRNA-seq clusters predicted that *Cdh4*+;*Ebf2*+ cells, but not *Emx2*+ cells, localize to the anatomic area where interscapular BAT later develops (Fig. 1E). The *Cdh4*+;*Ebf2*+ cell cluster was present at E12.5 and became more prominent at E13.5 (Fig. 1F). Immunostaining analysis identified cells co-expressing CDH4 and EBF2 proteins in the dorsal anterior region of embryos at E12.5 and E13.5 (Fig. 1G). Lineage tracing with *En1-Cre*; *Rosa26-Tdtomato* mice showed that cells expressing the DM marker *En1* gave rise to CDH4+ cells in the BAT-forming area at E13.5 (Fig. 1H). Overall, these results identify *Cdh4*+;*Ebf2*+ cells as presumptive early progenitors for brown adipocytes.

Dpp4+ mesenchymal cells contribute to adipocytes and fascial cells in BAT

Brown adipocytes appear between E13.5 and E15.5 (Fig. 1A, B)[18]. Integrated analysis of mesenchymal cells (*Pdgfra*+) and adipocytes localized in the dorsal-anterior region during this period identified several interesting cell clusters (Fig. 2A; Fig. S1–2). PreAds represent direct precursors of adipocytes; these cells express fibroblast markers such as *Pdgfra* and certain adipogenic genes, including *Pparg*, but do not express mature adipocyte genes such as *Adipoq* (Fig. 2A, B). At this stage, *Cdh4* and *Ebf2* were broadly expressed across several clusters, including *Cdh4*+;*Ngfr*+, *Cdh4*+;*Ngfr*− cells and an emergent population of cells marked by expression of dipeptidyl peptidase-4 (*Dpp4*) and peptidase inhibitor 16 (*Pi16*) (i.e. *Dpp4*+ cells). Tendon-associated cells were marked by expression of tenomodulin (*Tnmd*). Immunostaining analysis showed that NGFR expression was selective to fibroblasts enmeshed in developing skeletal muscle and were not present in developing BAT (Fig. 2C), implying that *Cdh4*+;*Ngfr*+ cells at this stage do not directly contribute to BAT development.

Dpp4+ cells neighbored PreAds in UMAP space and expressed low levels of *Pparg*, suggesting that these cells could function as progenitors for PreAds (Fig. 2A, B). Deconvolution analysis of MOSTA predicted that *Dpp4*+ cells localize tightly around developing adipocytes in BAT (Fig. 2D). Consistently, immunostaining analysis showed that DPP4+ cells reside in a thin layer of connective tissue fascia closely associated with, and surrounding, lobules of developing BAT (Fig. 2E). To determine if DPP4+ cells descend from *En1*-expressing cells, we performed lineage tracing using *En1-Cre*;*Tdtomato* reporter animals. Analysis of E14.5 embryos showed co-localization of TdTomato and DPP4 expression in fibroblastic cells surrounding BAT, as well as extensive labeling of BAT adipocytes with TdTomato (Fig. 2F). Altogether, these results suggest that the *En1*+ DM gives rise to brown adipocytes and BAT-associated connective tissue fascia.

To assess if *Dpp4*+ cells give rise to brown adipocytes, we performed lineage tracing analysis using *Dpp4*$^{Cre\text{-}ERT2}$; *TdTomato* reporter mice. Our previous studies demonstrated highly specific labeling of *Dpp4*+ cells using this mouse strain[21]. We induced TdTomato labeling of *Dpp4*-expressing cells by treating pregnant dams with tamoxifen at E13.5 or E14.5, corresponding to the period at which expression of *Dpp4* and other markers of *Dpp4*+ cells were first detected in the BAT-forming region. Immunostaining analysis of embryos at E16.5 showed that ~'20% of DPP4+ cells in the connective tissue surrounding BAT were labeled with TdTomato expression. We also observed TdTomato expression in a small but reproducible number of brown adipocytes (<1%), marked by PPARg expression (Fig. 2G). These results indicate that *Dpp4*+ cells have the capacity to contribute to fetal brown adipocyte development, but do not likely represent the main cellular source of brown adipocytes at this stage.

Identification of GATA6 as a marker of brown adipocyte progenitor cells

We analyzed the expression profiles of embryonic mesenchymal cells to search for novel regulators of brown adipocyte development. To this end, we generated a list of transcription factors that were selectively expressed in PreAds compared to all other fibroblast populations in the E13.5 to E15.5 datasets (Fig. 3A). *Gata6* was the 2nd highest ranking candidate gene on this list, immediately following the master adipogenic factor *Pparg* (Fig. 3A). Inspection of the scRNA-seq profiles showed *Gata6* expression in both PreAds and *Dpp4*+ cells (Fig. 3B). Immunostaining analysis of embryos showed that GATA6 expression was induced at E13.5 and strongly increased in developing BAT at E14.5 and E15.5 (Fig. 3C). Interestingly, GATA6 expression decreased in BAT adipocytes at E16.5 but was maintained in the DPP4+ fibroblasts surrounding BAT (Fig. 3C). To determine if *GATA6* is expressed during human brown adipocyte development, we analyzed an RNA sequencing (RNAseq) dataset from human iPSCs differentiated into brown adipocytes (GEO accession GSE131169)[22]. Analogous to the results in mice, GATA6 expression dramatically and transiently increased during the human brown adipocyte differentiation process, with its induction preceding the rise in *PPARg* expression (Fig. 3D). These results identify GATA6 as a candidate regulator of brown adipogenic commitment.

GATA6 is required for BAT development

Lastly, we investigated the functional role of GATA6 in brown adipocyte development. To do this, we deleted *Gata6* from the earliest stages of brown adipose lineage development by intercrossing *Myf5-Cre* and *Gata6* flox mice. *Myf5* is first expressed in the dermomyotome at E8, and *Myf5*-expressing cells give rise to skeletal muscle, BAT, and dorsal dermis[18,23]. Within the brown fat lineage, *Gata6* is expressed in PreAds and *Dpp4*+ cells, with no detectable expression in skeletal muscle. The resulting *Gata6*$^{\Delta Myf5}$ mutant mice were viable and displayed no obvious growth or developmental defects. Strikingly, mutant mice at P0 displayed a dramatic reduction, and in some animals, a complete loss, of interscapular BAT (Fig. 4A). At P0, *Gata6* mutant mice displayed a dose-dependent reduction in BAT weight, including a ~'70% reduction in homozygous mutant and ~'25% reduction in heterozygous mutant mice compared to littermate controls (Fig. 4B). *Gata6* mRNA levels were reduced/absent in the residual BAT of heterozygous and mutant animals (Fig. 4C). Interestingly, the residual BAT in *Gata6* mutant animals appeared normal and expressed relatively normal

levels of brown fat marker genes such as *Pparg2*, *Ucp1*, *Adipoq* and *Fabp4* (Fig. 4D). A severe reduction in BAT was also observed in 9-week-old adult *Gata6* mutant animals, suggesting that GATA6 is required for embryonic BAT development and postnatal BAT expansion (Fig. 4E).

To determine if GATA6 is required from the initial stages of BAT differentiation, we analyzed control and mutant embryos at E14.5. Immunostaining analysis showed a selective loss of GATA6 protein expression in the BAT forming region of mutant embryos (Fig. 4F). Strikingly, mutant embryos exhibited dramatically lower levels of PPARg protein expression and a severe reduction of developing brown adipocytes, compared to their littermate controls (Fig. 4F, Fig. S3). Immunostaining for DPP4 showed that the connective tissue surrounding *Gata6* mutant BAT, mainly composed of DPP4+ fibroblasts, was present in normal amounts and had a normal-appearing morphology. scRNA-seq analysis of dorsal anterior tissue from control and *Gata6* mutant embryos at E14.5 demonstrated a drastic reduction of adipogenic cells in the mutant embryos (Fig. S4). Interestingly, we did not detect major gene expression changes across other mesenchymal cell types.

To search for direct target genes of GATA6 in the brown adipose lineage, we performed chromatin immunoprecipitation (ChIP) sequencing analysis for GATA6 on dissected BAT from E15.5 embryos. *De novo* motif analysis of GATA6-binding sites identified a high enrichment of DNA binding motifs for EBF and c/EBP, which are important brown adipogenic transcription factors (Fig. 4G). GATA6 binding sites were found at many genes implicated in adipogenesis (Fig. 4H). This includes a prominent binding peak, correlating with high levels of H3K27-acetylation at the promoter region of the key BAT transcription factor *Ebf2*. We also observed GATA6 binding and high levels of H3K27-acetylation at the promoter regions of *Ctcf*, *Tcf3, and Ak1*, encoding proteins implicated in adipogenesis[24–28]. Altogether, these findings suggest that GATA6 cooperates with EBF2 and c/EBP transcription factors to promote PreAd commitment upstream of *Pparg* expression.

Discussion

BAT is a key thermogenic organ that helps animals maintain body temperature during cold exposure. BAT activity is also linked with protection against obesity and metabolic complications. While the physiological role of BAT in suppressing weight gain or regulating metabolism is debated, especially in humans, there is general agreement that increasing BAT activity has the potential to counteract obesity and related disease. A recent study also implicates a role for BAT in suppressing cancer growth[5]. Thus, a detailed understanding of BAT development may reveal new approaches to increase BAT content for reducing obesity and other diseases.

The interscapular BAT depot descends from the paraxial mesoderm, which also gives rise to other cell types, including skeletal muscle, bone, cartilage and dermis[13–16,18,19]. Our study provides a comprehensive profile of the mesenchymal cell types that contribute to the development of BAT and related lineages. An important feature of our study was the application of a spatial temporal atlas of gene expression in embryos, enabling us to separate out cell types unrelated to BAT development and refine the analysis based on the localization

of identified cell types. We found that committed preadipocytes, expressing fibroblast and adipogenic genes, emerge between E13.5 and E14.5 of development, immediately followed by the induction of brown adipocytes. Prior to E15.5, adipocytes are only found in BAT depots, with white adipocytes developing after birth. However, progenitor and/or preadipocyte cells for white adipocytes that share a common gene signature with brown progenitor cells may be present at this stage.

At earlier embryonic stages, we identified a presumptive early progenitor population for preadipocytes, marked by the expression of *Cdh4* and the brown adipose lineage factor *Ebf2*. *Cdh4*+;*Ebf2*+ cells descend from the *En1*-expressing DM and localize in the dorsal anterior region of embryos at E12.5 to E13.5, just before the emergence of *Pparg*+ cells. Future lineage tracing studies will be needed to ascertain if *Cdh4*+;*Ebf2*+ cells give rise to preadipocytes and/or other cell types.

We also identified a distinct population of fibroblasts, marked by the expression of *Dpp4* and *Pi16* that appeared at the onset of BAT differentiation and were located in close proximity to PreAds in UMAP space. Immunostaining and spatial transcriptomic analysis indicated that these cells constitute the connective tissue fascia that surrounds and presumably provides a scaffold for developing brown adipocytes. Our analysis of the MOSTA predicted that *Dpp4*+ cells constitute a fascial tissue layer that extends along the dorsal aspect of the embryo. Whether there are molecular or functional differences between the DPP4+ cells in different regions remains unclear. Our previous studies identified a transcriptionally similar DPP4+ fibroblast population in perivascular adipose tissue (PVAT) and adult fat depots[21,29,30]. Lineage tracing analyses in adult mice show that *Dpp4*+ cells contribute to adipocyte turnover and adipocyte expansion in a depot-selective manner, with high levels of adipogenic contribution in visceral relative to subcutaneous WAT depots [21]. In the current study, we found that embryonic *Dpp4*+ cells contribute, but in a limited way, to brown adipocyte development. We conclude that *Dpp4*+ cells are not a major source of embryonic brown adipocytes. Rather, we speculate that *Dpp4*+ cells are competent for adipogenesis and that some of these cells, located in specific locations, undergo adipocyte differentiation upon encountering very strong adipogenic stimuli in the context of developing BAT. We further posit that *Dpp4*+ cells may function as a reserve progenitor compartment, contributing to adipocyte formation when preadipocyte cells are exhausted or impaired.

This study also highlights the co-development of BAT fascia and adipogenic cells, possibly originating from the same progenitor cells (Fig. 4I). Notably, *DPP4* and *PPARg* expression both increased at similar time points during the differentiation of human iPSCs into brown adipocytes, suggesting that fascial cells and brown adipocytes also co-develop in humans. Of note, our dataset also identified a population of skeletal muscle-associated connective tissue cells, marked by the expression of *Ngfr*. The DPP4+ fascial cells around BAT express high levels of various extracellular matrix components, including *Fbn1* and *Mfap5*, which presumably play important roles in providing structural support for BAT and may regulate adipocyte differentiation. These cells also secrete paracrine factors with the potential to regulate BAT development and function. An obvious candidate is *Bmp7*, which is highly and specifically expressed in DPP4+ cells and plays a critical role in driving brown adipocyte differentiation[31,32].

GATA6 also plays a critical role in the development of other organs, including heart, liver, pancreas, intestine, and lung[33–38]. Among mesenchymal cells in the mesoderm/BAT lineage, *Gata6* expression was selective to PreAds and *Dpp4*+ cells. Moreover, GATA6 expression increased during the intense period of adipogenesis between E13.5 and E16.5, with its expression declining thereafter, and becoming restricted to DPP4+ cells and other fibroblastic cells. ChIP studies suggest that GATA6 cooperates with the brown adipogenic transcription factors EBF and c/EBP to promote adipogenic commitment. Interestingly, we identified a prominent binding site for GATA6 at the EBF2 promoter, suggesting that GATA6 regulates EBF2 expression to drive brown fat differentiation.

Deletion of *Gata6* in the brown fat lineage resulted in a striking loss of PPARg expression and brown adipocyte development. The BAT deficit in mutant animals was apparent from the earliest stages of *Pparg* induction and adipocyte differentiation at E14.5 and persisted into adulthood. scRNA-seq analysis at E14.5 revealed a selective loss of *Pparg*+ PreAds in *Gata6* mutant embryos without major shifts in the gene expression profile of other related fibroblast populations. Notably, the requirement for GATA6 in BAT development distinguishes it from other known transcriptional regulators of BAT (i.e. EBF2, PRDM16), which control BAT vs. WAT specific character, but are not required for adipocyte differentiation[39–41]. These results suggest that GATA6 regulates adipogenic commitment upstream of *Pparg* induction.

The small amount of residual BAT present in some *Gata6* mutant animals exhibited a normal morphology and molecular profile. Importantly, *Gata6* mRNA expression was decreased to background levels and the *Gata6* locus was recombined at the DNA level in mutant BAT. These results indicate that the small number of adipocytes in mutant BAT do not derive from a separate lineage. It is conceivable that a related GATA family member compensates for loss of GATA6, though the most highly related factor, GATA4 is not well expressed in PreAds or DPP4+ cells. Alternatively, GATA6 may regulate the sensitivity of progenitor cells to certain adipogenic cue(s), such that some cells (i.e., those very close to the signal source), may reach the signaling threshold that triggers adipogenesis in the absence of GATA6. Further studies are needed to clarify the mechanism-of-action of GATA6 in brown adipogenic cells.

In summary, these studies reveal a proposed lineage hierarchy for BAT adipocyte and connective tissue cells, beginning with the DM and progressing through CDH4+/EBF2+ cells, followed by GATA6-expressing preadipocytes (Fig. 4I). We further identify GATA6 as a critical transcriptional regulator of brown adipocyte development. This information can be applied to develop and improve iPSC-based protocols to generate human brown adipocytes for transplantation and functional analysis. Future studies focused on GATA6 may also reveal novel methods to promote brown adipogenic commitment and expand BAT mass.

Limitations of the study

Our study strongly implicates CDH4+/EBF2+ cells as progenitor cells for brown preadipocytes based on their transcriptional signature and their emergence in the BAT-forming region preceding the development of preadipocytes. However, lineage-tracing analysis is necessary to conclusively determine the function of CDH4+/EBF2+

cells, including their contribution to BAT development. Additionally, while our study demonstrates that GATA6 is required for the development of brown preadipocytes, the mechanism of GATA6 action remains uncertain. Our results suggest that GATA6 promotes the expression of *Pparg* and other adipogenic factors to drive the transition of CDH4+/EBF2+ cells into preadipocytes. However, additional or alternative roles for GATA6 should be considered, including regulation of preadipocyte proliferation and/or survival, and/or regulation of the BAT microenvironment.

STAR Methods

Resource availability

Lead contact—Further information and requests for resources and reagents should be directed to and will be fulfilled by the lead contact, Patrick Seale (sealep@pennmedicine.upenn.edu).

Materials availability—This study did not generate new unique reagents.

Data and code availability—Single-cell RNA-seq and ChIP-seq data have been deposited at GEO under the accession number GSE233955. Any additional information required to reanalyze the data reported in this paper is available from the lead contact upon request. Microscopy data reported in this paper will be shared by the lead contact upon request.

Experimental model and subject details

Mice—All animal experiments were performed according to procedures approved by the University of Pennsylvania's Institutional Animal Care and Use Committee (approval no. 805649). Mice were housed under the care of University of Pennsylvania University Laboratory Animal Resources. Mice were raised at room temperature with a 12-h light–dark cycle and fed a regular chow diet (LabDiet, 5010). Timed-pregnant CD-1 IGS mice (CD-1, Charles River) and *Ebf2*^{GFP} knock-in mice[42] were used for the E10.5 to E15.5 scRNA-seq. Timed-pregnant Swiss Webster mice (CFW, Charles River) and CD-1 IGS mice (CD-1, Charles River) were used for embryo immunostaining experiments. For embryonic lineage tracing, timed matings were set up at night and plugs checked in the morning (E0.5). Tamoxifen (Sigma, T5648; stock 20 mg ml–1 in corn oil) was administered to dams intraperitoneally at a dose of 150 mg kg–1 in the morning. Embryos were collected for analysis on the morning of the specified day. Experiments performed on embryonic and perinatal mice were conducted on male and female mice. *Gata6* mutant mice were generated by crossing *Myf5-Cre* knock-in mice (Jackson Labs, Strain #007893)[43] with *Gata6* floxed animals (Jackson Labs, Strain# 008196)[44]. For lineage tracing studies, *En1-Cre* (Jackson Labs strain #007916)[45] or *Dpp4-CreER* mice[21] were crossed with *R26R-tdTomato* (Ai14) reporter mice (Jackson Labs, Strain#007914). For chromatin immunoprecipitation (ChIP) experiments, CD-1 IGS mice (CD-1, Charles River) were used for timed mating and harvested at E15.5. Experiments at adult time points were performed in male and female mice between the ages of 9 to 18 weeks.

Method details

Histology and Immunofluorescence—Tissues were fixed in 4% paraformaldehyde overnight, washed in PBS, dehydrated in ethanol, paraffin-embedded and sectioned. Following deparaffinization, slides were subjected to heat antigen retrieval in a pressure cooker with Bulls Eye Decloaking buffer (Biocare), unless otherwise noted. Slides were incubated in primary antibody overnight and secondary antibody conjugated to peroxidase and then developed using Tyramide Signal Amplification (TSA, Akoya Biosciences). Images were captured on a Leica TCS SP8 confocal microscope, Leica Stellaris or Keyence BZ-X700 fluorescent light microscope.

RNA Extraction, qRT-PCR and RNA Sequencing—Total RNA was extracted using TRIzol (Invitrogen) combined with Purelink RNA columns (Fisher) and quantified using a Nano-drop. mRNA was reverse transcribed to cDNA using the ABI High-Capacity cDNA Synthesis kit (ABI). Real-time PCR was performed on a QuantStudio5 qPCR machine using SYBR green fluorescent dye (Applied Biosystems). Fold changes were calculated using the ddCT method, with TATA binding Protein (*Tbp*) mRNA serving as a normalization control. We analyzed an RNAseq dataset from a differentiation time course of human iPSC-to-brown adipocytes (GEO accession GSE131169)[22].

Generation of single cell suspensions from mouse embryos.: For the E10.5 to E15.5 scRNA-seq time-course, embryos were collected at the specified time points and heads and limbs were removed. The dorsal upper back portion was minced and digested with either 0.25% trypsin (Fisher) or Collagenase D: 6.1 mg ml–1 (Roche) and Dispase II: 2.4 mg ml–1 (Roche). Samples were placed at 37 °C with constant agitation (200 r.p.m), followed by quenching for 30 min with an equal volume of complete medium (DMEM/10% FBS). Dissociated cells were suspended using a P1000 pipette and filtered through a 100 μm filter. Cells were pelleted at 400g for 4 min, and red blood cells were lysed in 155 mM NH4Cl, 12 mM NaHCO3 and 0.1 mM EDTA for 4 min. An equal volume of complete medium was added, and the cells were filtered through a 40 μm filter for downstream analyses. Isolated cells were suspended in FACS buffer (HBSS, 3% 0.45 μM filtered FBS; Thermo Fisher). Cells were stained in FACS buffer with antibodies for 1 h at 4 °C in the dark. Cells were washed twice with cold FACS buffer and sorted on a FACS Aria cell sorter (BD Biosciences) with a 100 μm nozzle. All compensation was performed at the time of acquisition in BD FACS DIVA software (8.0.1) using single stained cells and compensation beads. Downstream analysis and visualization of flow data were performed in FlowJo (10.6.2). For the control and *Gata6*$^{\Delta Myf5}$ mutant embryos at E14.5, dorsal anterior tissue at the forelimb level was dissected and spinal cord and ribs were removed as much as possible. Tissue from each embryo was individually minced and digested with Type I Collagenase: 0.6mg ml–1 (Worthington Biochemical Corp) and Dispase II: 2.4mg ml–1 (Roche). Samples were placed at 37 °C for 45min, vortexed every 15 min and quenched with complete medium (DMEM/10% FBS). Filtering and lysis were done as described above. To verify the mutants, tails from each embryo were lysed with Proteinase K (Fisher) and Lysis buffer to extract DNA and PCR was done using GoTaq Green PCR Master mix (CC-Promega) and *Myf5-cre* primer (PCR protocol from Jackson Labs, Strain #007893). 5

control embryos and 6 mutant embryos were separately pooled in FACS buffer, followed by staining and flow sorting as described above.

scRNA-seq samples.: For the E10.5 to E15.5 time-course, single cells were flow sorted to isolate live (DAPI(−)) cells and remove debris. We enriched for mesenchymal, DM and brown adipose lineage cells as follows. (i) E11.5 and E12.5 DM and mesenchymal cells based on cell surface expression of PDGFRa and/or LRIG1 [30% PDGFRa+, LRIG1(−) cells; 25% PDGFRa(−), LRIG1+ cells, 30% PDGFRa+, LRIG1+ cells, 15% PDGFRa(−), LRIG1(−) cells]. (ii) E13.5-E15.5 fibroblasts through selection of PDGFRa+ cells [75% PDGFRa+; 25% PDGFRa(−)]. (iii) E10.5, E14.5, and E15.5 brown adipose lineage cells based on expression of *Early B Cell Factor-2* (*Ebf2*)-*GFP* [75% *Ebf2*-GFP+; 25% *Ebf2*-GFP(−)][18]. The selection of *Lrig1*, *Pdgfra* and *Ebf2* as marker genes of mesenchymal cells was informed through analysis of a mouse organogenesis cell atlas[46], showing that *Lrig1* was co-expressed with the DM marker *En1*, *Pdgfra* was broadly expressed in mesenchymal cells, and *Ebf2* was expressed in a subset of mesenchymal cells designated as the “connective tissue trajectory”. Single cell libraries were prepared using a Chromium Single Cell 3’ Reagent Kit (Version 3) and sequenced on an Illumina HiSeq 4000 or an Illumina NovaSeq 6000 by the University of Pennsylvania Next Gen Sequencing Core or CHOP Center for Applied Genomics Sequencing Core. For the control and $Gata6^{\Delta Myf5}$ mutant embryos at E14.5, live (DAPI(−)) cells were flow sorted. Single cell libraries were prepared using Chromium Next GEM Single Cell 3’ v3.1 with Dual Index and sequenced on Illumina NovaSeq6000 by CHOP High Throughput Sequencing Core. Reads were aligned using Cell Ranger[47].

scRNA-seq analysis

Analysis of individual embryonic stages.: Single-cell RNA-seq analysis was performed using Seurat v4[48]. For the E10.5 to E15.5 time-course, cutoffs for the minimum number of unique genes detected (1200–2500) and the maximum percentage of reads mapping to mitochondrial genes (7–15%) were determined individually for each individual dataset, such that no clusters in downstream analysis were defined by low-quality cells. Doublets were computationally predicted using Scrublet[49] and excluded from further analysis. Gene counts were log-normalized, and regression was performed using the ScaleData function for the following variables: percentage of reads mapping to mitochondrial genes, percentage of reads mapping to histone genes, and cell cycle phase (G2M.Score/S.Score as calculated by the CellCycleScoring function). After principal component analysis (PCA), dimensional reduction was performed using UMAP, and clusters were defined using the FindNeighbors and FindClusters functions. For the control and $Gata6^{\Delta Myf5}$ mutant embryos at E14.5, cells were filtered out if they had fewer than 500 or more than 2500 genes detected, more than 7000 counts, or greater than 3.5% of reads mapping to mitochondrial genes.

Data integration.: For the E10.5 to E15.5 time-course, cell clusters corresponding to fibroblasts and/or skeletal muscle were selected from each embryonic stage based on expression of *Pdgfra* and *Tnnt1*, respectively (Fig. S1A). Cells from individual embryonic stages were integrated to produce datasets representing E10.5-E13.5 fibroblasts and skeletal muscle (“E10.5-E13.5 Mesenchyme”) or E13.5-E15.5 fibroblasts and adipocytes (“E13.5-

E15.5 Mesenchyme") (Fig. S1A). Resulting cell clusters predicted to localize to the dorsal mouse embryo (see "Spatial Deconvolution Analysis" section) were selected and re-analyzed for further analysis ("E10.5-E13.5 Dorsal Mesenchyme" and "E13.5-E15.5 Dorsal Mesenchyme"). Finally, clusters from the "Dorsal Mesenchyme" datasets not marked by *Pax1* (sclerotome) or *Tnmd* (tendon) were integrated to produce the E10.5-E15.5 "Proposed brown adipose lineage" dataset (Fig. S1A). For both the E10.5 to E15.5 time-course and control and *Gata6*$^{\Delta Myf5}$ mutant embryos at E14.5, integration was performed using reciprocal PCA as implemented in Seurat v4. Downstream analyses were performed as for the individual datasets. Cluster-defining genes were determined using the FindAllMarkers function.

Spatial Deconvolution Analysis.: Spatial transcriptomics datasets generated from sagittal slices of E10.5-E15.5 mouse embryos were downloaded from the Mouse Organogenesis Spatial Transcriptomics Atlas (MOSTA)[20]. To create a robust reference for cell-type deconvolution of the spatial transcriptomics data, cells included in the "E10.5-E13.5 Mesenchyme" and "E13.5-E15.5 Mesenchyme" datasets were supplemented with endothelial, cardiac, hematopoietic, neuronal, neural crest, and epithelial cells that had been excluded from mesenchymal cell analysis. Cell-type deconvolution of spatial transcriptomic data was then performed using SpaDecon[50]. The "E10.5-E13.5 Mesenchyme" dataset was used to deconvolve MOSTA data corresponding to E10.5, E11.5, E12.5, or E13.5; the "E13.5-E15.5 Mesenchyme" dataset was used to deconvolve MOSTA data corresponding to E13.5, E14.5, or E15.5 (Fig.S1A).

Identification of preadipocyte-enriched transcription factors.: Genes enriched in preadipocytes (PreAd group in "E13.5-E15.5 Dorsal Mesenchyme" dataset) versus all other groups were identified using the FindMarkers function in Seurat. Transcription factors were selected from the list of enriched genes based on a list of murine transcription factors downloaded from TcoF-DB v2 (https://tools.sschmeier.com/tcof/home/)[51].

Chromatin Immunoprecipitation (ChIP) and ChIP-Sequencing Analysis.: Dissected embryonic interscapular BAT pads were pooled and approximately 65 mg of tissue was fixed with 1% methanol-free formaldehyde for 10 min. After quenching, nuclei were isolated using a hypotonic buffer and Kimble dounce homogenizer. Nuclei were lysed in SDS buffer and chromatin was sonicated using an Active Motif EpiShear at 20% amplitude for 3 min with cycles of 15 sec ON 20 sec OFF to obtain fragments ranging from 200–600 bp. Fragmented chromatin was incubated with 1 μg of antibody overnight at 4 °C and bound to protein A/G magnetic beads for pull-down. ChIP-seq libraries were prepared using the KAPA HyperPrep Kit and library barcodes were from the KAPA Unique Dual-Index kit. Libraries were amplified using 10 cycles on the thermocycler. Post amplification libraries were cleaned up using Agencourt AMPure XP beads from Beckman Coulter. Libraries were validated by Azenta/Genewiz with Agilent Tapestation.

Quantification and Statistical Analysis—Statistical details for each experiment are described in the corresponding figure legends. Biological replicates (number of animals) are denoted as 'n'. Graphpad Prism software was used to perform statistical analyses. For

statistical analyses, a minimum of 5 biological replicates per group were used. Values are presented as mean ± standard error of the mean. Holm-Sidak multiple correction was used to determine the statistical differences between samples. Significant differences are represented in the legends as follows: *p<0.05, **p<0.01, ***p<0.001; ****p<0.0001.

Supplementary Material

Refer to Web version on PubMed Central for supplementary material.

Acknowledgements

We thank Dr. Lori Sussel and Dr. Yana Kamberov for providing mouse strains. We also thank Dr. Amin Abedini, Dr. Konstantin Kloetzer and Dr. Katalin Susztak for preparation of single cell sequencing libraries. This work was supported by NIH grants DK123356, AR078650, DK120982 to P.S, DK120062 to A.R.A., T32DK007314 to E.C.F., T32GM008216 to A.P.S, DK116922 to R.R.S., 40–45200-98–21118 to J.M.E.T. (The Netherlands Organisation for Health Research and Development) and P30-DK19525 (Penn Diabetes Research Center).

Inclusion and diversity

One or more of the authors of this paper self-identifies as an underrepresented ethnic minority in science.

References

1. Cannon B, and Nedergaard J (2004). Brown adipose tissue: function and physiological significance. Physiological reviews 84, 277–359. [PubMed: 14715917]
2. Enerback S, Jacobsson A, Simpson EM, Guerra C, Yamashita H, Harper ME, and Kozak LP (1997). Mice lacking mitochondrial uncoupling protein are cold-sensitive but not obese. Nature 387, 90–94. 10.1038/387090a0.
3. Cohen P, and Kajimura S (2021). The cellular and functional complexity of thermogenic fat. Nature reviews. Molecular cell biology 22, 393–409. 10.1038/s41580-021-00350-0. [PubMed: 33758402]
4. Sakers A, De Siqueira MK, Seale P, and Villanueva CJ (2022). Adipose-tissue plasticity in health and disease. Cell 185, 419–446. 10.1016/j.cell.2021.12.016. [PubMed: 35120662]
5. Seki T, Yang Y, Sun X, Lim S, Xie S, Guo Z, Xiong W, Kuroda M, Sakaue H, Hosaka K, et al. (2022). Brown-fat-mediated tumour suppression by cold-altered global metabolism. Nature 608, 421–428. 10.1038/s41586-022-05030-3. [PubMed: 35922508]
6. Cypess AM, Lehman S, Williams G, Tal I, Rodman D, Goldfine AB, Kuo FC, Palmer EL, Tseng YH, Doria A, et al. (2009). Identification and importance of brown adipose tissue in adult humans. N Engl J Med 360, 1509–1517. [PubMed: 19357406]
7. Ouellet V, Routhier-Labadie A, Bellemare W, Lakhal-Chaieb L, Turcotte E, Carpentier AC, and Richard D (2011). Outdoor temperature, age, sex, body mass index, and diabetic status determine the prevalence, mass, and glucose-uptake activity of 18F-FDG-detected BAT in humans. J Clin Endocrinol Metab 96, 192–199. 10.1210/jc.2010-0989. [PubMed: 20943785]
8. Saito M, Okamatsu-Ogura Y, Matsushita M, Watanabe K, Yoneshiro T, Nio-Kobayashi J, Iwanaga T, Miyagawa M, Kameya T, Nakada K, et al. (2009). High incidence of metabolically active brown adipose tissue in healthy adult humans: effects of cold exposure and adiposity. Diabetes 58, 1526–1531. [PubMed: 19401428]
9. van Marken Lichtenbelt WD, Vanhommerig JW, Smulders NM, Drossaerts JM, Kemerink GJ, Bouvy ND, Schrauwen P, and Teule GJ (2009). Cold-activated brown adipose tissue in healthy men. N Engl J Med 360, 1500–1508. [PubMed: 19357405]
10. Virtanen KA, Lidell ME, Orava J, Heglind M, Westergren R, Niemi T, Taittonen M, Laine J, Savisto NJ, Enerback S, and Nuutila P (2009). Functional brown adipose tissue in healthy adults. N Engl J Med 360, 1518–1525. [PubMed: 19357407]

11. Lidell ME, Betz MJ, Dahlqvist Leinhard O, Heglind M, Elander L, Slawik M, Mussack T, Nilsson D, Romu T, Nuutila P, et al. (2013). Evidence for two types of brown adipose tissue in humans. Nat Med 19, 631–634. 10.1038/nm.3017. [PubMed: 23603813]
12. Aherne W, and Hull D (1966). Brown adipose tissue and heat production in the newborn infant. J Pathol Bacteriol 91, 223–234. 10.1002/path.1700910126. [PubMed: 5941392]
13. Atit R, Sgaier SK, Mohamed OA, Taketo MM, Dufort D, Joyner AL, Niswander L, and Conlon RA (2006). Beta-catenin activation is necessary and sufficient to specify the dorsal dermal fate in the mouse. Developmental biology 296, 164–176. [PubMed: 16730693]
14. Lepper C, and Fan CM (2010). Inducible lineage tracing of Pax7-descendant cells reveals embryonic origin of adult satellite cells. Genesis 48, 424–436. [PubMed: 20641127]
15. Sanchez-Gurmaches J, Hung CM, Sparks CA, Tang Y, Li H, and Guertin DA (2012). PTEN loss in the Myf5 lineage redistributes body fat and reveals subsets of white adipocytes that arise from Myf5 precursors. Cell Metab 16, 348–362. [PubMed: 22940198]
16. Seale P, Bjork B, Yang W, Kajimura S, Chin S, Kuang S, Scime A, Devarakonda S, Conroe HM, Erdjument-Bromage H, et al. (2008). PRDM16 controls a brown fat/skeletal muscle switch. Nature 454, 961–967. [PubMed: 18719582]
17. Sebo ZL, Jeffery E, Holtrup B, and Rodeheffer MS (2018). A mesodermal fate map for adipose tissue. Development 145. 10.1242/dev.166801.
18. Wang W, Kissig M, Rajakumari S, Huang L, Lim HW, Won KJ, and Seale P (2014). Ebf2 is a selective marker of brown and beige adipogenic precursor cells. Proc Natl Acad Sci U S A 111, 14466–14471. 10.1073/pnas.1412685111. [PubMed: 25197048]
19. Wang W, and Seale P (2016). Control of brown and beige fat development. Nature reviews. Molecular cell biology 17, 691–702. 10.1038/nrm.2016.96. [PubMed: 27552974]
20. Chen A, Liao S, Cheng M, Ma K, Wu L, Lai Y, Qiu X, Yang J, Xu J, Hao S, et al. (2022). Spatiotemporal transcriptomic atlas of mouse organogenesis using DNA nanoball-patterned arrays. Cell 185, 1777–1792 e1721. 10.1016/j.cell.2022.04.003. [PubMed: 35512705]
21. Stefkovich M, Traynor S, Cheng L, Merrick D, and Seale P (2021). Dpp4+ interstitial progenitor cells contribute to basal and high fat diet-induced adipogenesis. Mol Metab 54, 101357. 10.1016/j.molmet.2021.101357. [PubMed: 34662714]
22. Zhang L, Avery J, Yin A, Singh AM, Cliff TS, Yin H, and Dalton S (2020). Generation of Functional Brown Adipocytes from Human Pluripotent Stem Cells via Progression through a Paraxial Mesoderm State. Cell stem cell 27, 784–797 e711. 10.1016/j.stem.2020.07.013. [PubMed: 32783886]
23. Ott MO, Bober E, Lyons G, Arnold H, and Buckingham M (1991). Early expression of the myogenic regulatory gene, myf-5, in precursor cells of skeletal muscle in the mouse embryo. Development 111, 1097–1107. 10.1242/dev.111.4.1097. [PubMed: 1652425]
24. Mikkelsen TS, Xu Z, Zhang X, Wang L, Gimble JM, Lander ES, and Rosen ED (2010). Comparative epigenomic analysis of murine and human adipogenesis. Cell 143, 156–169. 10.1016/j.cell.2010.09.006. [PubMed: 20887899]
25. Li J, Yu X, Pan W, and Unger RH (2002). Gene expression profile of rat adipose tissue at the onset of high-fat-diet obesity. American journal of physiology. Endocrinology and metabolism 282, E1334–1341. 10.1152/ajpendo.00516.2001. [PubMed: 12006364]
26. Hilgendorf KI, Johnson CT, Mezger A, Rice SL, Norris AM, Demeter J, Greenleaf WJ, Reiter JF, Kopinke D, and Jackson PK (2019). Omega-3 Fatty Acids Activate Ciliary FFAR4 to Control Adipogenesis. Cell 179, 1289–1305 e1221. 10.1016/j.cell.2019.11.005. [PubMed: 31761534]
27. Cristancho AG, Schupp M, Lefterova MI, Cao S, Cohen DM, Chen CS, Steger DJ, and Lazar MA (2011). Repressor transcription factor 7-like 1 promotes adipogenic competency in precursor cells. Proc Natl Acad Sci U S A 108, 16271–16276. 10.1073/pnas.1109409108. [PubMed: 21914845]
28. Chen Y, He R, Han Z, Wu Y, Wang Q, Zhu X, Huang Z, Ye J, Tang Y, Huang H, et al. (2022). Cooperation of ATF4 and CTCF promotes adipogenesis through transcriptional regulation. Cell Biol Toxicol 38, 741–763. 10.1007/s10565-021-09608-x. [PubMed: 33950334]
29. Angueira AR, Sakers AP, Holman CD, Cheng L, Arbocco MN, Shamsi F, Lynes MD, Shrestha R, Okada C, Batmanov K, et al. (2021). Defining the lineage of thermogenic perivascular adipose tissue. Nat Metab 3, 469–484. 10.1038/s42255-021-00380-0. [PubMed: 33846639]

30. Merrick D, Sakers A, Irgebay Z, Okada C, Calvert C, Morley MP, Percec I, and Seale P (2019). Identification of a mesenchymal progenitor cell hierarchy in adipose tissue. Science 364. 10.1126/science.aav2501.

31. Schulz TJ, Huang P, Huang TL, Xue R, McDougall LE, Townsend KL, Cypess AM, Mishina Y, Gussoni E, and Tseng YH (2013). Brown-fat paucity due to impaired BMP signalling induces compensatory browning of white fat. Nature 495, 379–383. 10.1038/nature11943. [PubMed: 23485971]

32. Tseng YH, Kokkotou E, Schulz TJ, Huang TL, Winnay JN, Taniguchi CM, Tran TT, Suzuki R, Espinoza DO, Yamamoto Y, et al. (2008). New role of bone morphogenetic protein 7 in brown adipogenesis and energy expenditure. Nature 454, 1000–1004. [PubMed: 18719589]

33. Beuling E, Aronson BE, Tran LM, Stapleton KA, ter Horst EN, Vissers LA, Verzi MP, and Krasinski SD (2012). GATA6 is required for proliferation, migration, secretory cell maturation, and gene expression in the mature mouse colon. Mol Cell Biol 32, 3392–3402. 10.1128/MCB.00070-12. [PubMed: 22733991]

34. Carrasco M, Delgado I, Soria B, Martin F, and Rojas A (2012). GATA4 and GATA6 control mouse pancreas organogenesis. J Clin Invest 122, 3504–3515. 10.1172/JCI63240. [PubMed: 23006330]

35. Keijzer R, van Tuyl M, Meijers C, Post M, Tibboel D, Grosveld F, and Koutsourakis M (2001). The transcription factor GATA6 is essential for branching morphogenesis and epithelial cell differentiation during fetal pulmonary development. Development 128, 503–511. 10.1242/dev.128.4.503. [PubMed: 11171334]

36. Xuan S, Borok MJ, Decker KJ, Battle MA, Duncan SA, Hale MA, Macdonald RJ, and Sussel L (2012). Pancreas-specific deletion of mouse Gata4 and Gata6 causes pancreatic agenesis. J Clin Invest 122, 3516–3528. 10.1172/JCI63352. [PubMed: 23006325]

37. Xuan S, and Sussel L (2016). GATA4 and GATA6 regulate pancreatic endoderm identity through inhibition of hedgehog signaling. Development 143, 780–786. 10.1242/dev.127217. [PubMed: 26932670]

38. Zhao R, Watt AJ, Li J, Luebke-Wheeler J, Morrisey EE, and Duncan SA (2005). GATA6 is essential for embryonic development of the liver but dispensable for early heart formation. Mol Cell Biol 25, 2622–2631. 10.1128/MCB.25.7.2622-2631.2005. [PubMed: 15767668]

39. Angueira AR, Shapira SN, Ishibashi J, Sampat S, Sostre-Colon J, Emmett MJ, Titchenell PM, Lazar MA, Lim HW, and Seale P (2020). Early B Cell Factor Activity Controls Developmental and Adaptive Thermogenic Gene Programming in Adipocytes. Cell reports 30, 2869–2878 e2864. 10.1016/j.celrep.2020.02.023. [PubMed: 32130892]

40. Harms MJ, Ishibashi J, Wang W, Lim HW, Goyama S, Sato T, Kurokawa M, Won KJ, and Seale P (2014). Prdm16 is required for the maintenance of brown adipocyte identity and function in adult mice. Cell Metab 19, 593–604. 10.1016/j.cmet.2014.03.007. [PubMed: 24703692]

41. Rajakumari S, Wu J, Ishibashi J, Lim HW, Giang AH, Won KJ, Reed RR, and Seale P (2013). EBF2 determines and maintains brown adipocyte identity. Cell Metab 17, 562–574. 10.1016/j.cmet.2013.01.015. [PubMed: 23499423]

42. Wang SS, Lewcock JW, Feinstein P, Mombaerts P, and Reed RR (2004). Genetic disruptions of O/E2 and O/E3 genes reveal involvement in olfactory receptor neuron projection. Development 131, 1377–1388. 10.1242/dev.01009. [PubMed: 14993187]

43. Tallquist MD, Weismann KE, Hellstrom M, and Soriano P (2000). Early myotome specification regulates PDGFA expression and axial skeleton development. Development 127, 5059–5070. [PubMed: 11060232]

44. Sodhi CP, Li J, and Duncan SA (2006). Generation of mice harbouring a conditional loss-of-function allele of Gata6. BMC developmental biology 6, 19. 10.1186/1471-213X-6-19. [PubMed: 16611361]

45. Kimmel RA, Turnbull DH, Blanquet V, Wurst W, Loomis CA, and Joyner AL (2000). Two lineage boundaries coordinate vertebrate apical ectodermal ridge formation. Genes Dev 14, 1377–1389. [PubMed: 10837030]

46. Cao J, Spielmann M, Qiu X, Huang X, Ibrahim DM, Hill AJ, Zhang F, Mundlos S, Christiansen L, Steemers FJ, et al. (2019). The single-cell transcriptional landscape of mammalian organogenesis. Nature 566, 496–502. 10.1038/s41586-019-0969-x. [PubMed: 30787437]

47. Zheng GX, Terry JM, Belgrader P, Ryvkin P, Bent ZW, Wilson R, Ziraldo SB, Wheeler TD, McDermott GP, Zhu J, et al. (2017). Massively parallel digital transcriptional profiling of single cells. Nat Commun 8, 14049. 10.1038/ncomms14049. [PubMed: 28091601]

48. Hao Y, Hao S, Andersen-Nissen E, Mauck WM 3rd, Zheng S, Butler A, Lee MJ, Wilk AJ, Darby C, Zager M, et al. (2021). Integrated analysis of multimodal single-cell data. Cell 184, 3573–3587 e3529. 10.1016/j.cell.2021.04.048. [PubMed: 34062119]

49. Wolock SL, Lopez R, and Klein AM (2019). Scrublet: Computational Identification of Cell Doublets in Single-Cell Transcriptomic Data. Cell Syst 8, 281–291 e289. 10.1016/j.cels.2018.11.005. [PubMed: 30954476]

50. Coleman K, Hu J, Schroeder A, Lee EB, and Li M (2023). SpaDecon: cell-type deconvolution in spatial transcriptomics with semi-supervised learning. Commun Biol 6, 378. 10.1038/s42003-023-04761-x. [PubMed: 37029267]

51. Schmeier S, Alam T, Essack M, and Bajic VB (2017). TcoF-DB v2: update of the database of human and mouse transcription co-factors and transcription factor interactions. Nucleic acids research 45, D145–D150. 10.1093/nar/gkw1007. [PubMed: 27789689]

Highlights

- scRNA-seq of embryonic mesoderm identifies BAT lineage cells and related cell types.
- *Dpp4*-expressing cells form the connective tissue that encases developing BAT.
- The transcription factor GATA6 marks BAT progenitor cells.
- GATA6 is required for PPARg expression induction and brown preadipocyte development.

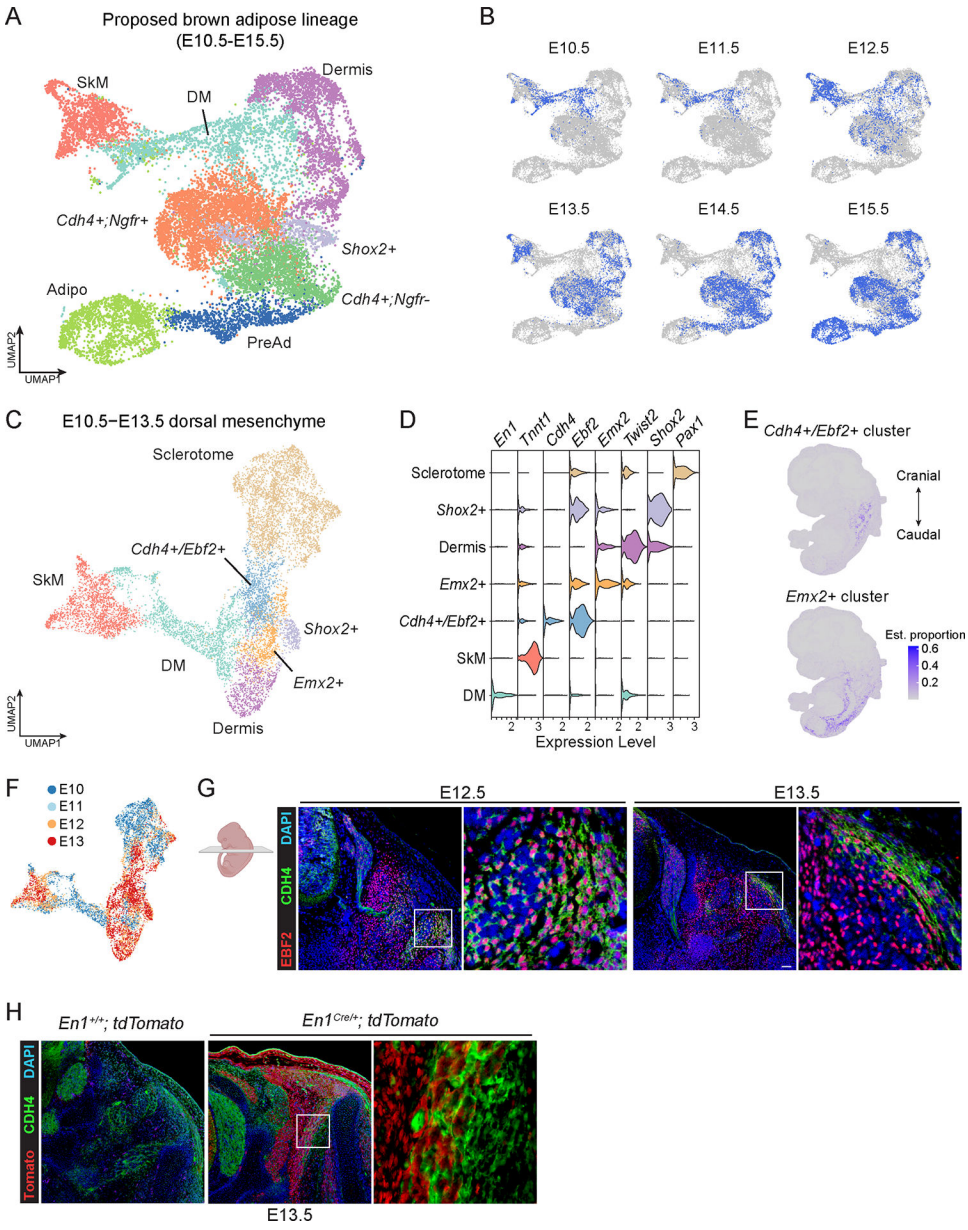

Figure 1. Profiling of mesenchymal cells during brown adipose tissue (BAT) development

(A) Uniform manifold approximation and projection (UMAP) of 16,165 cells related to the dermomyotome-brown adipose lineage based on marker gene expression and computationally predicted anatomic location (see workflow in Fig. S1).

(B) Cells in (A) highlighted by developmental stage of origin.

(C) UMAP of 9,895 mesenchymal and skeletal muscle cells from E10.5-E13.5 mouse embryos, representing clusters predicted to localize to the dorsal mouse embryo, where BAT develops (see Fig. S1). Clusters marked by *Pax1* expression were aggregated into the Sclerotome group.

(D) Violin plots corresponding to (C).

(E) Cells in (C) were incorporated into a reference used to deconvolve spatial gene expression data from an E12.5 embryo. Color intensity indicates the estimated proportion of cells at each spot corresponding to the given cell type.

(F) Cells in (C) colored by developmental stage of origin.

(G) Schematic for cross-section in the anterior region of embryo (created with Biorender.com; left) and immunostaining of CDH4 (green) and EBF2 (red) in the anterior region of mouse embryos at E12.5 and E13.5 (n=3 each, scale bar, 100 μm; right). NT = Neural tube.

(H) Immunostaining of CDH4 (green) and tdTomato (red) in the anterior region of E13.5 embryo from *En1*$^{+/+}$; tdTom (control) and *En1*$^{Cre/+}$; tdTom reporter mice. (n=2 Cre−; n=3 Cre+, scale bar, 100 μm) NT = Neural tube.

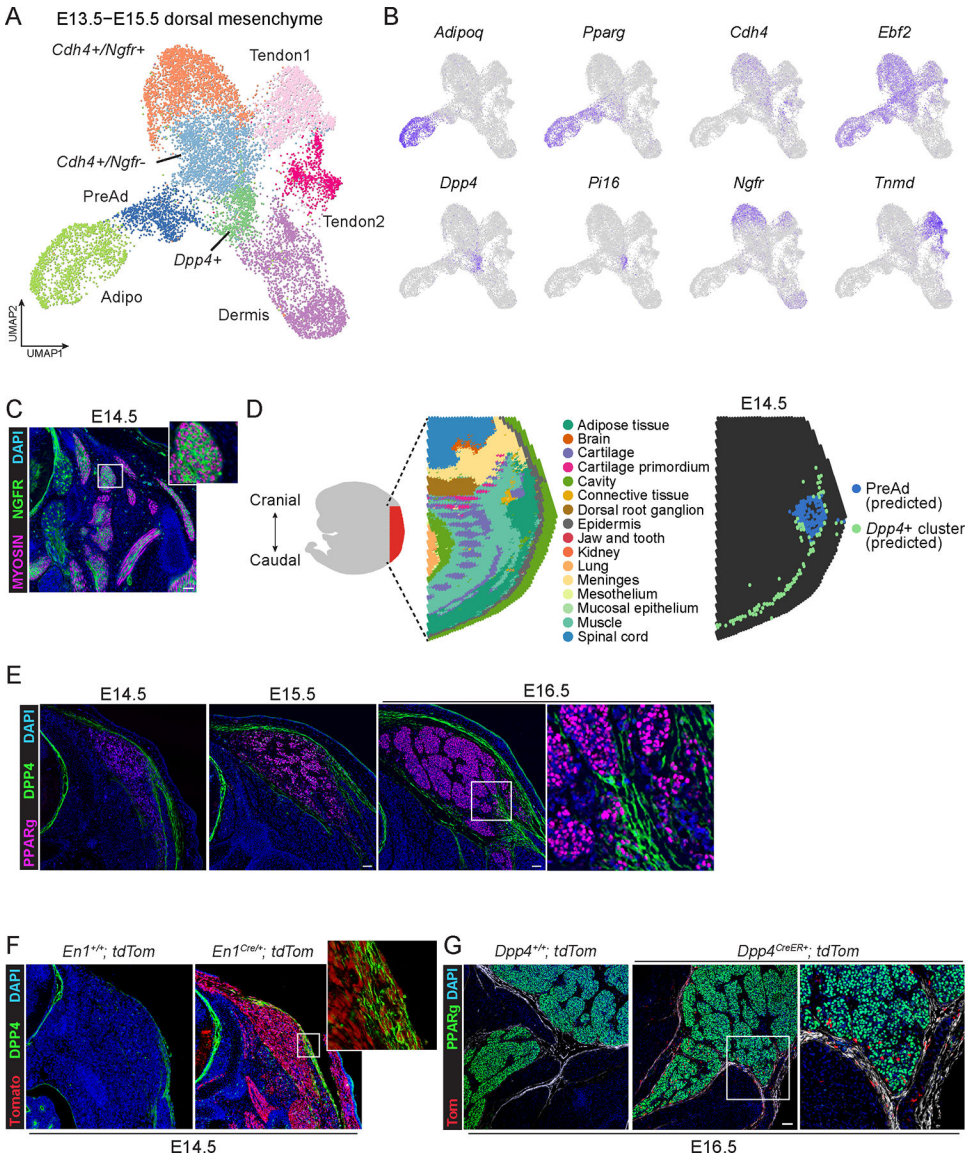

Figure 2. DPP4+ mesenchymal cells contribute to adipocytes and fascial cells in BAT

(A) UMAP of 13,474 mesenchymal cells from E13.5-E15.5 mouse embryos, representing clusters predicted to localize to the dorsal mouse embryo, where BAT develops (also see Fig. S1).

(B) Expression of marker genes in cells from (A).

(C) Immunostaining of NGFR (green) and MYOSIN (magenta) in the anterior region of mouse embryos at E14.5. (n=3, scale bar, 100 μm) NT = Neural tube

(D) Mesenchymal cells from E13.5-E15.5 were incorporated into a reference used to deconvolve spatial gene expression data from an E14.5 embryo. (Left) Segment of spatial gene expression data used for deconvolution. (Center) Atlas-provided annotations of spots [20]. (Right) Blue or green spots indicate where PreAds or *Dpp4*+ cells are predicted to make up >40% or >10% of cells, respectively.

(E) Immunostaining of DPP4 (green) and PPARg (magenta) in the anterior region of mouse embryos at E14.5 to E16.5. (n=11 E14.5; n=4 E15.5; n=4 E16.5, scale bar, 100 μm). NT = Neural tube.

(F) Immunostaining of DPP4 (green) and tdTomato (red) in the anterior region of E14.5 embryo from *En1*$^{+/+}$*; tdTom* (control) and *En1*$^{Cre/+}$; tdTom reporter mice. (n=3 Cre−; n=9 Cre+, scale bar, 100 μm). NT = Neural tube.

(G) Immunostaining of PPARg (green), DPP4 (white) and tdTomato (red) in the anterior region of E16.5 embryo from *Dpp4*$^{+/+}$*; tdTom* (control) and *Dpp4*$^{CreER/+}$*; tdTom* reporter mice. (n=4 Cre−; n=10 Cre+, scale bar, 100 μm). NT = Neural tube.

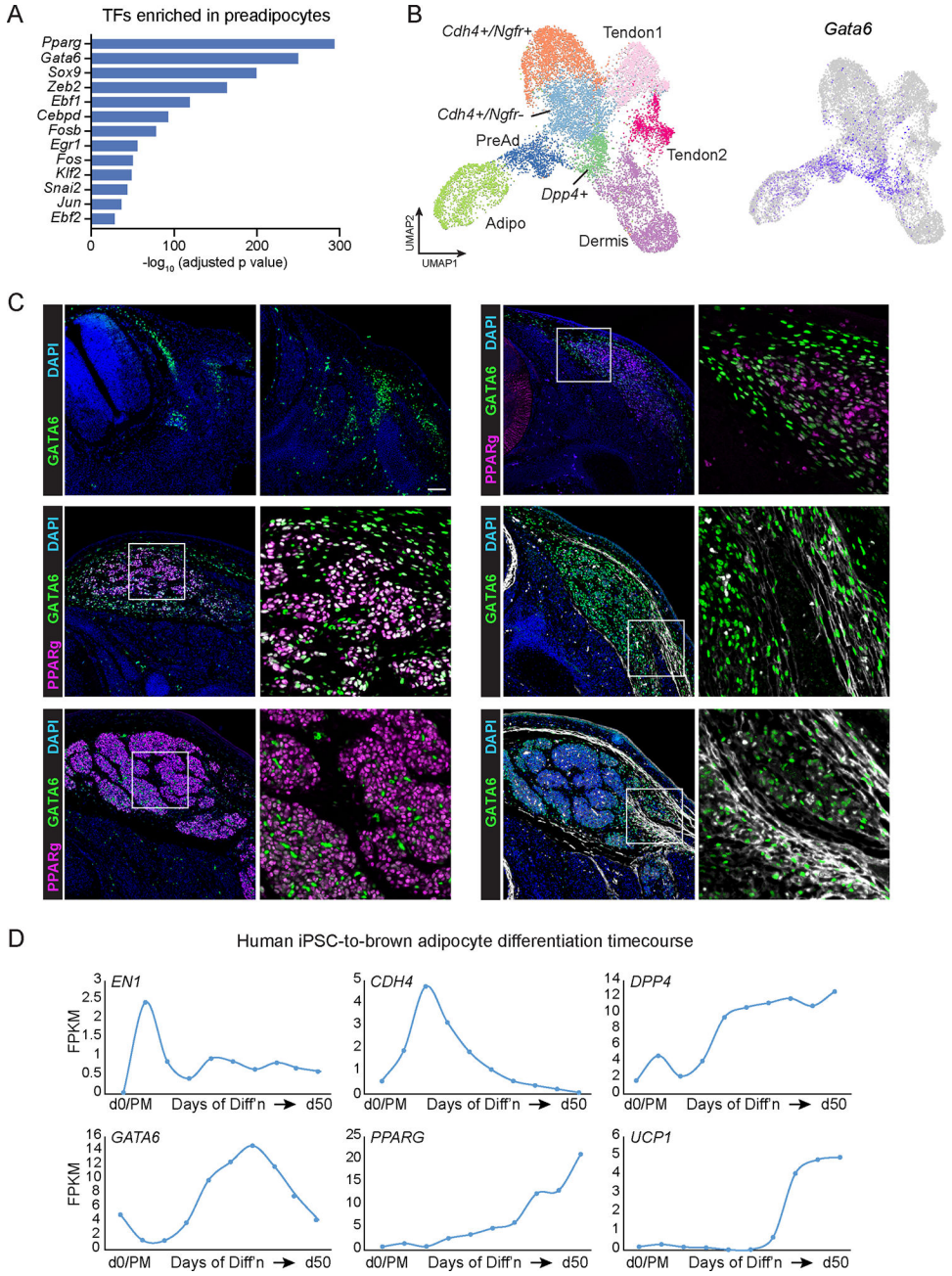

Figure 3. Identification of GATA6 as a marker of brown adipocyte progenitor cells

(A) Transcription factors enriched in preadipocytes relative to all other E13.5-E15.5 dorsal mesenchyme cell clusters ($log_2FC > 0.25$). *P* values were calculated using the FindMarkers function in Seurat.

(B) UMAP (left) and *Gata6* expression (right) in E13.5-E15.5 dorsal mesenchymal cells (see Fig. 2A).

(C) Immunostaining of GATA6 (green), PPARg (magenta), and DPP4 (white) in the anterior region of mouse embryos from E12.5 to E16.5. (n=3 E12.5; n=3 E13.5; n=6 E14.5; n=6 E15.5, n=5 E16.5; scale bar, 100 μm) NT = Neural tube.

(D) mRNA expression levels of indicated genes during human iPSC-to-brown adipocyte differentiation.

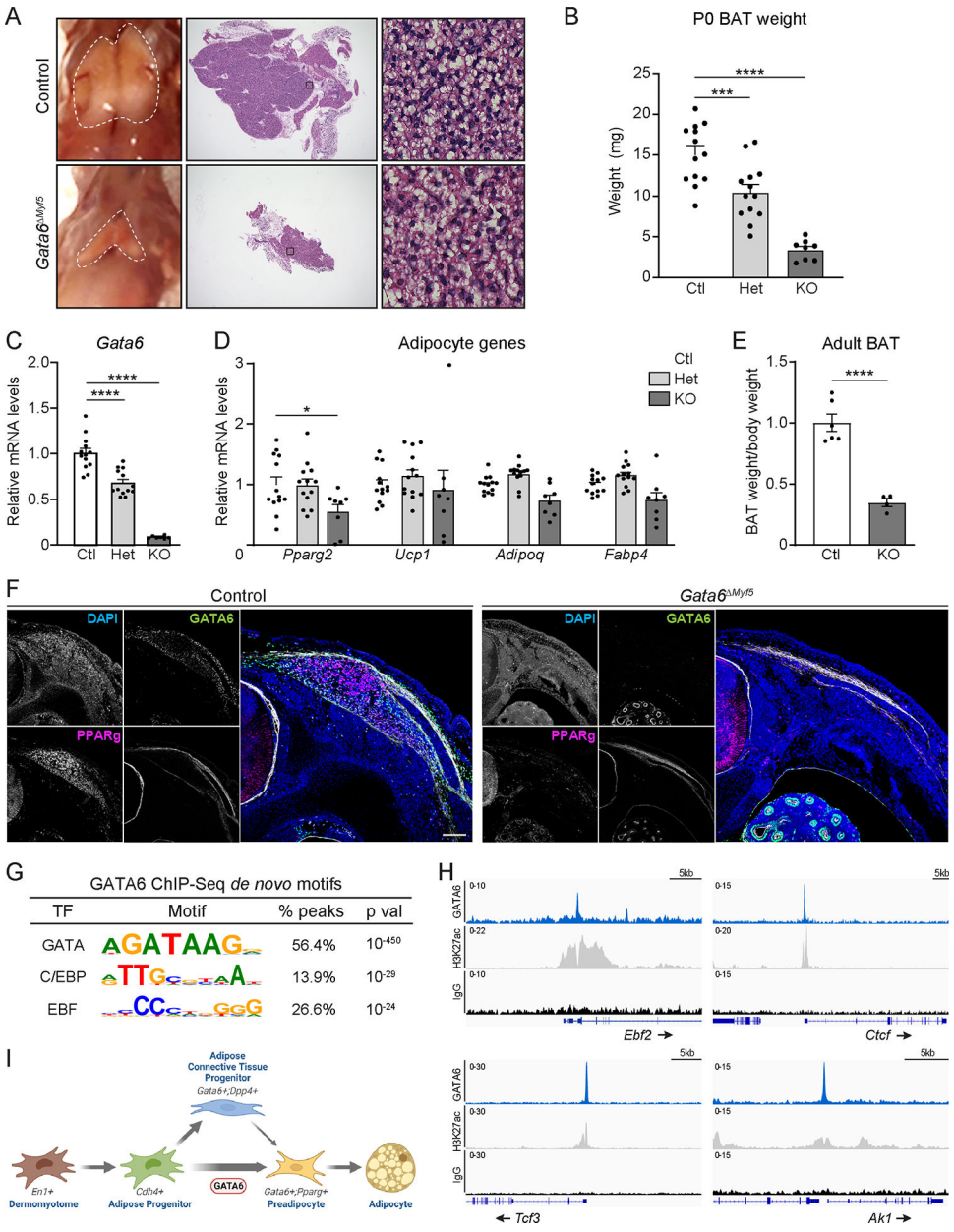

Figure 4. GATA6 is required for BAT development

(A) Macroscopic view and H&E staining of interscapular BAT from *Myf5*$^{+/+}$;*Gata6*$^{fl/fl}$ (control) and *Myf5*$^{Cre/+}$;*Gata6*$^{fl/fl}$ (homozygous mutant, *Gata6*$^{\Delta Myf5}$) mice at P0. BAT is highlighted by dashed lines. (n=5 Ctl; n=7 KO, scale bar, 200 μm)

(B) BAT weight of the control, *Myf5*$^{Cre/+}$;*Gata6*$^{fl/+}$ (heterozygous mutant) and *Gata6*$^{\Delta Myf5}$ mice at P0 (n=8 Ctl; n=13 Het, n=13 KO, mean ± s.e.m.). One-way ANOVA followed by all pairwise comparisons with Holm-Sidak multiple correction. ***P≤ 0.001, ****P≤ 0.0001.

(C) *Gata6* mRNA levels in interscapular BAT from control, heterozygous and homozygous mutant mice at P0 (n=8 Ctl; n=13 Het; n=13 KO, mean ± s.e.m.). One-way ANOVA followed by all pairwise comparisons with Holm-Sidak multiple correction. ****P≤ 0.0001.

(D) mRNA levels of BAT-selective genes in BAT from control and *Gata6*$^{\Delta Myf5}$ mice at P0 (n=8 Ctl; n=13 Het; n=13 KO, mean ± s.e.m.). One-way ANOVA followed by all pairwise comparisons with Holm-Sidak multiple correction. *P≤ 0.05.

(E) Weights of interscapular BAT from control and *Gata6*$^{\Delta Myf5}$ adult mice (normalized by body weight) (n=6 Ctl; n=4 KO, mean ± s.e.m.). Two-sample, two-sided t-test. ****P≤ 0.0001.

(F) Immunostaining of GATA6 (green), PPARg (magenta) and DPP4 (white) in the anterior region of control and *Gata6*$^{\Delta Myf5}$ mice at E14.5. (n=11 Ctl; n=11 KO, scale bar, 100 μm). NT = Neural tube.

(G) *De novo* motif analysis of GATA6-binding regions in E15.5 BAT.

(H) ChIP-seq profiles in reads per million total reads (RPM) for GATA6 (blue), H3K27-Ac (gray), and IgG (black) in E15.5 BAT at the following genes: *Ebf2, Ctcf, Tcf3, Ak1.*

(I) Working model of the brown adipocyte lineage hierarchy, highlighting the role of GATA6 in regulating brown adipogenic commitment upstream of *Pparg* expression.

Key resources table

REAGENT or RESOURCE	SOURCE	IDENTIFIER
Antibodies		
Goat anti-PDGFRalpha	R and D Systems, AF1062	RRID:AB_2236897
Sheep anti-EBF-2	R and D Systems, AF7006	RRID:AB_10972102
Goat anti-GATA-6	R and D Systems, AF1700	RRID:AB_2108901
Rabbit anti-Perilipin (D418)	Cell Signaling, 3470	RRID:AB_2167268
Rabbit anti-PPAR gamma (K.242.9)	Thermo Fisher, MA5–14889	RRID:AB_10985650
Goat anti-DPPIV/CD26	R and D Systems, AF954	RRID:AB_355739
Sheep anti-Cadherin-4	R and D Systems, AF6677	RRID:AB_10890570
Anti-PDGFRα-PECy7	Biolegend, 135912	RRID:AB_2715974
Goat anti-LRIG1	R and D Systems, AF3688	RRID:AB_2138836
Donkey anti-goat Alexa 488	Invitrogen, A11055	RRID:AB_2534102
Anti-human/mouse CD271 (LNGFR)	Miltenyi Biotec, 130–122-980	RRID:AB_2811422
Mouse anti-Myosin Heavy Chain	R and D Systems, MAB4470	RRID:AB_1293549
Rabbit anti-GATA-6 (used in Figure 4)	Cell Signaling, 5851S	RRID:AB_10705521
Rabbit anti-H3K27ac	Active Motif, 39133	RRID:AB_2561016
Rabbit IgG	Cell Signaling, 2729S	RRID:AB_1031062
Chemicals, peptides, and recombinant proteins		
Tamoxifen (Free Base)	Sigma	Cat#T5648
Corn Oil	Sigma	Cat#C8267
16% Paraformaldehyde	Electron Microscopy Sciences	Cat#15710
TRIzol	Invitrogen	Cat#15596018
DAPI	Sigma	Cat#D9542
Collagenase D	Roche	Cat#11088858001
Type I Collagenase	Worthington Biochemical Corp	Cat#LS004197
Dispase II	Roche	Cat#4942078001
Proteinase K	Fisher	Cat#BP1700100
Critical commercial assays		
ABI High-Capacity cDNA Synthesis kit	Applied Biosystems	Cat#4368813
Purelink RNA Mini columns	Invitrogen	Cat#LT-12183018
TSA TMR Tyramide Reagent Pack	Akoya Biosciences	Cat#NEL742001KT
TSA Fluorescein Tyramide Reagent Pack	Akoya Biosciences	Cat#NEL741001KT
ChIP-grade Protein A/G Magnetic Beads	Pierce/Thermo Scientific	Cat#26162
Bulls Eye Decloaking Buffer	Biocare	Cat#BULL1000 MX
AbC Total Antibody Compensation Kit	BioLegend	Cat#A10497
Agencourt AMPure XP beads	Beckman Coulter	Cat#A63880
GoTaq Green PCR Master Mix	CC-Promega	Cat#M7123
Chromium Single Cell 3' Reagent Kit (Version 3)	10x Genomics	Cat#CG000183

REAGENT or RESOURCE	SOURCE	IDENTIFIER
Chromium Next GEM Single Cell 3' v3.1 with Dual Index	10x Genomics	Cat#CG000315
KAPA HyperPrep with Library Amplification	Roche	Cat#KK8502
KAPA Unique Dual-Indexed Adapters	Roche	Cat#KK8726
Deposited data		
scRNA-seq data (this study)	Gene Expression Omnibus	GSE233955
ChIP-seq data (this study)	Gene Expression Omnibus	GSE233955
Human iPSC-BA RNA-seq	Gene Expression Omnibus	GSE131169 Zhang, et al. (2020)[22]
Mouse Organogenesis Spatial Transcriptomics Atlas (MOSTA)	China National GeneBank (https://db.cngb.org/stomics/mosta/download/)	Chen, et al. (2022)[20]
Experimental models: Organisms/strains		
Myf5^{Cre}	The Jackson Laboratory	RRID:IMSR_JAX:007893
Rosa26 loxp-stop-loxp tdTomato (Ai14)	The Jackson Laboratory	RRID:IMSR_JAX:007914
Gata6$^{flox/flox}$	The Jackson Laboratory	RRID:IMSR_JAX:008196
En1^{Cre}	The Jackson Laboratory	RRID:IMSR_JAX:007916
Dpp4^{CreER}	Seale Laboratory	Stefkovich, et al. (2021)[21]
Ebf2^{GFP} knock-in mice	Reed Laboratory	Wang, et al. (2004)[42]
CFW (Swiss Webster)	Charles River	RRID:IMSR_CRL:024
CD1 (Adult)	Charles River	RRID:IMSR_CRL:022
Oligonucleotides		
See Table S1	N/A	N/A
Software and algorithms		
FlowJo (10.6.2)	FlowJo	RRID:SCR_008520
Seurat (4.1.1)	Satija Lab (https://satijalab.org/seurat/index.html)	RRID:SCR_016341
Scrublet (0.2.3)	Bioconda (https://anaconda.org/bioconda/scrublet)	RRID:SCR_018098
RStudio (2022.07.1)	RStudio (https://www.rstudio.com/)	RRID:SCR_000432
GraphPad Prism 9	GraphPad (https://www.graphpad.com/scientific-software/prism/)	RRID:SCR_002798
tidyverse (1.3.1)	CRAN (https://cran.r-project.org/web/packages/tidyverse/index.html)	RRID:SCR_019186
ggplot2 (3.3.6.9000)	CRAN (https://cran.r-project.org/web/packages/ggplot2/index.html)	RRID:SCR_014601
SpaDecon (1.1.1)	PyPi (https://pypi.org/project/SpaDecon/)	Coleman, et al. (2023)[50]
R (4.1.1)	R Foundation (https://www.r-project.org/)	RRID:SCR_001905
Other		
Active Motif EpiShear (Sonicator)	Active Motif	Cat#53051
HiSeq 4000	Illumina	N/A
NovaSeq 6000	Illumina	N/A
BZ X700 Microscope	Keyence	N/A
SP8 Microscope	Leica	N/A

REAGENT or RESOURCE	SOURCE	IDENTIFIER
Stellaris Microscope	Leica	N/A